Journal of Fluids and Structures (1999) **13,** 209–224
Article No.: jfls.1998.0199 available online at http://www.idealibrary.com on IDEAL

NUMERICAL INVESTIGATIONS OF THE AERODYNAMICS AND THE AEROELASTIC STABILITY OF OSCILLATING ANNULAR WINGS

A. KNIPFER

Institute of Aeroelasticity, DLR Göttingen, Germany

(Received 6 March 1998 and in revised form 9 October 1998)

The nacelles of modern aeroengines are constantly increasing in size. Thus, engine air-loads are becoming more powerful and their importance for the aeroelastic stability is becoming more significant. The principal goal of this study is to answer the question of how unsteady airloads vary while shifting to transonic Mach numbers. The investigations are carried out by applying a finite volume Euler method to a harmonically oscillating annular wing. The results show that transonic effects in the case of an annular wing are essentially weaker than in the case of an airfoil. The order of magnitude of the variations is around 10%. Possible consequences for the aeroelastic stability are examined with the example of an elastically mounted annular wing in transonic flow. The shifts of the stability curves also remain within a range of 10%. In addition, an actuator disk method, which is frequently used for the simulation of the fan jet, is expanded in such a way that unsteady flows can be treated. Some unsteady air-loads are strongly dependent on the pressure jump across the fan.

1. INTRODUCTION

1.1. OUTLINE

THE BYPASS RATIOS OF MODERN AEROENGINES are within a range of 4 to 6. Manufactures are on the verge of developing aeroengines having bypass ratios of 10 to 20. The corresponding nacelles take on enormous dimensions, compared to earlier generations of engines. Accordingly, engine air-loads are becoming more powerful and their importance for the aeroelastic stability of the aeroplane is increasing. Thus, it is necessary to become more familiar with the unsteady aerodynamics of an oscillating nacelle. In the present study, the aerodynamics of the annular wing is investigated as a first step towards more complete configurations.

From airfoil theory, it is a well-known fact that unsteady air-loads can vary greatly while shifting to transonic Mach numbers. The principal goal of this study is to examine whether the annular wing exhibits the same high sensitivity of the air-loads to Mach number variations.

All numerical calculations have been done utilizing Euler's equations. This implies that the results are inexact in the flow regime where separation occurs. However, from an aeroelastic point of view, the costs of a complete 3-D Navier–Stokes solution still seem too high because of the high number of reduced frequencies and Mach numbers that have to be included in an aeroelastic stability survey. Taking viscous effects into account is left to future investigations.

0889–9746/99/020209 + 16 $30.00

1.2. Definition

The annular wing is assumed to be stiff. It can exhibit pitch oscillations,

$$\alpha(t) = \alpha_0 \cos(\omega t), \tag{1}$$

or heave oscillations in the z-direction with amplitude z_0,

$$z(t) = z_0 \cos(\omega t). \tag{2}$$

The geometrical situation is pictured in Figure 1.

This motion causes a normal force F_N and a moment M about the middle axis A. The force coefficient c_N and c_M are defined as follows:

$$c_N = \frac{F_N}{\frac{1}{2}\rho_\infty U_\infty^2 DL}, \quad c_M = \frac{M}{\frac{1}{2}\rho_\infty U_\infty^2 DL^2}; \tag{3, 4}$$

ρ_∞ and U_∞ are the density and velocity of the fluid far away from the annular wing; L and D are the length and the diameter of the annular wing, respectively.

If the amplitudes are small, a harmonic time dependence of $c_N(t)$ and $c_M(t)$ is a good approximation:

$$c_N(t) = c'_N \cos(\omega t) - c''_N \sin(\omega t), \tag{5}$$

$$c_M(t) = c'_M \cos(\omega t) - c''_M \sin(\omega t). \tag{6}$$

The unsteady air-load coefficients c'_N, c''_N, c'_M and c''_M are usually denoted as the real and imaginary parts of the normal force and moment; the prime means the real and the double-prime the imaginary part, respectively. For small oscillations, these coefficients are proportional to the amplitude of the oscillation. Therefore, the results are usually expressed in the differential form

$$c_{N/M,\alpha} = \frac{\partial c_{N/M}}{\partial \alpha_0}, \quad c_{N/M,z} = \frac{L}{2}\frac{\partial c_{N/M}}{\partial z_0}, \tag{7, 8}$$

In this study, α_0 is always 1^0 and z_0/L equals 0·01.

The most important parameters are the aspect ratio $\Lambda = D/L$; the reduced frequency $\omega^* = \omega L/U_\infty$; and the Mach number Ma_∞.

1.3. State of the Research

Steady calculations have been done by several authors for potential flow (Weissinger 1956) or solving the complete Euler or Navier–Stokes equations (e.g. Ronzheimer 1989; Rudnik 1991; Hirose *et al.* 1991; Bolms & Schwamborn 1994).

Unsteady calculations have been made only by a few authors. These calculations utilized linear approximations and, therefore, could not treat transonic flows. The reason for this lies in the great computational effort needed to solve the full nonlinear equations. The required computer performance has been obtainable only since the last decade. Some results of these linear calculations are outlined in this section.

First, some steady results of the linearized potential theory are presented. An expanded lifting line theory (Weissinger 1956) yields this approximate expression for the normal force in incompressible flow:

$$c_N = \frac{\Lambda \pi^2 \alpha}{\Lambda + \pi/2 + \tan^{-1}(1{\cdot}2/\Lambda)}. \tag{9}$$

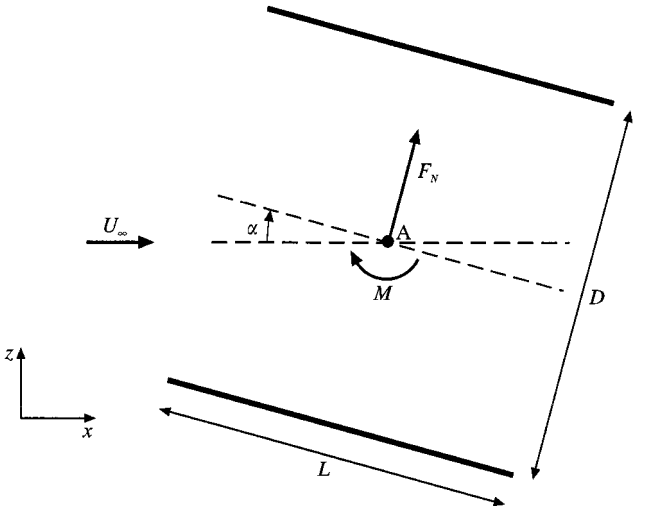

Figure 1. Oscillating annular wing (cross-section).

Applying the similarity rules for compressible flow [e.g. Schlichting & Truckenbrodt (1969)], we have

$$c_N = \frac{\Lambda\pi^2\alpha}{\beta\Lambda + \pi/2 + \tan^{-1}(1{\cdot}2/(\Lambda\beta))}, \tag{10}$$

with

$$\beta = \sqrt{1 - \mathrm{M}a_\infty^2}. \tag{11}$$

Thus, for Λ small enough, the Mach number dependence of the normal force is much weaker than in the case of the high aspect ratio airfoil, where the loads scale with $1/\beta$. In the limit of $\Lambda = 0$, they are completely independent of the Mach number. This result is the same as obtained by slender-body theory. The latter says that the lift should be independent of the Mach number also in transonic flow. In this paper, it shall be tested whether or not this is also true for an annular wing with $\Lambda = 1$.

The unsteady results can be summarized as follows. Potential flow theory yields the following lowest-order dependencies (Laschka 1964; Katzer 1989) for the unsteady air-loads in incompressible flow ($\mathrm{M}a_\infty = 0$):

$c'_{N,\alpha} \propto \Lambda$, $c''_{N,\alpha} \propto \Lambda\omega^*$, $c'_{M,\alpha} \propto \Lambda$, $c''_{M,\alpha} \propto -\Lambda$, $c'_{N,z} \propto \Lambda\omega^{*2}$, $c''_{N,z} \propto -\Lambda\omega^*$,

$c'_{M,z} \approx 0$ and $c''_{M,\alpha} \propto -\Lambda\omega^*$.

In order to compute the influence of the Mach number in subsonic flow, Angelini *et al.* (1974) used a doublet-lattice method. Their results indicate a slight increase of the unsteady load coefficients with the Mach number. A panel method, applied by Send (1989), yielded the same behaviour.

2. FUNDAMENTAL EQUATIONS

The fluid is assumed to be ideal. Therefore, the viscous terms can be neglected and the flow can be described by Euler's equations

$$\frac{\partial \mathbf{q}}{\partial t} + \frac{\partial \mathbf{f}}{\partial x} + \frac{\partial \mathbf{g}}{\partial y} + \frac{\partial \mathbf{h}}{\partial z} = \mathbf{0}. \tag{12}$$

The conservative variables $\mathbf{q}$ and the flux vectors $\mathbf{f}$, $\mathbf{g}$, and $\mathbf{h}$ are defined as follows:

$$\mathbf{q} = \begin{Bmatrix} \rho \\ \rho u \\ \rho v \\ \rho w \\ \rho E \end{Bmatrix}, \quad \mathbf{f} = \begin{Bmatrix} \rho u \\ \rho u^2 + p \\ \rho uv \\ \rho uw \\ \rho uI \end{Bmatrix},$$

$$\mathbf{g} = \begin{Bmatrix} \rho v \\ \rho uv \\ \rho v^2 + p \\ \rho vw \\ \rho vI \end{Bmatrix}, \quad \mathbf{h} = \begin{Bmatrix} \rho w \\ \rho uw \\ \rho vw \\ \rho w^2 + p \\ \rho wI \end{Bmatrix}; \tag{13}$$

ρ is the fluid density, p the static pressure, and $(u, v, w) = \mathbf{u}$ are the three components of the velocity in the x-, y- and z-direction. E is the total energy and I the total enthalpy per unit mass,

$$E = \frac{1}{\kappa - 1}\frac{p}{\rho} + \frac{1}{2}\mathbf{u}^2, \tag{14}$$

$$I = \frac{\kappa}{\kappa - 1}\frac{p}{\rho} + \frac{1}{2}\mathbf{u}^2. \tag{15}$$

κ is the adiabatic coefficient, which equals 7/5 for two-atom gases.

By quasilinear transformations, Euler's equations can be transformed into the characteristic form. This is needed in order to formulate the boundary conditions at the fan inlet and outlet.

$$\left(\frac{\partial}{\partial t} + \mathbf{u}\cdot\nabla\right)s_1 = 0, \tag{16}$$

$$\left(\frac{\partial}{\partial t} + \mathbf{u}\cdot\nabla\right)s_2 + \frac{1}{\rho}\mathbf{n}_1^{\perp}\cdot\nabla p = 0, \tag{17}$$

$$\left(\frac{\partial}{\partial t} + \mathbf{u}\cdot\nabla\right)s_3 + \frac{1}{\rho}\mathbf{n}_2^{\perp}\cdot\nabla p = 0, \tag{18}$$

$$\left(\frac{\partial}{\partial t} + (\mathbf{u} + a\mathbf{n})\cdot\nabla\right)s_4 + a\mathbf{t}(\mathbf{t}\cdot\nabla)\mathbf{u} = 0, \tag{19}$$

$$\left(\frac{\partial}{\partial t} + (\mathbf{u} - a\mathbf{n})\cdot\nabla\right)s_5 + a\mathbf{t}(\mathbf{t}\cdot\nabla)\mathbf{u} = 0, \tag{20}$$

with $\mathbf{n}_1^{\perp} = (-n_z, 0, n_x)$, and $\mathbf{n}_2^{\perp} = (n_y, -n_x, 0,)$, a is the speed of sound. The abbreviation $\mathbf{t}(\mathbf{t}\cdot\nabla)$ means $\mathbf{t}_1(\mathbf{t}_1\cdot\nabla) + \mathbf{t}_2(\mathbf{t}_2\cdot\nabla)$, where $\mathbf{n}$, $\mathbf{t}_1$ and $\mathbf{t}_2$ form a system of orthonormal basis vectors. The variations of the characteristic variables $s_{1,\ldots,5}$ are

$$\delta s_1 = \delta\rho - \frac{1}{a^2}\delta p, \tag{21}$$

$$\delta s_2 = \mathbf{n}_1^{\perp}\cdot\delta\mathbf{u}, \quad \delta s_3 = \mathbf{n}_2^{\perp}\cdot\delta\mathbf{u}, \tag{22, 23}$$

$$\delta s_4 = \mathbf{n}\cdot\delta\mathbf{u} + \frac{1}{\rho a}\delta p, \quad \delta s_5 = -\mathbf{n}\cdot\delta\mathbf{u} + \frac{1}{\rho a}\delta p. \tag{24, 25}$$

3. NUMERICAL METHODS

In this section, the numerical methods are introduced briefly. More information about the methods and the validation runs can be found in Knipfer (1995).

The five equations (12) are solved approximately utilizing a finite-volume algorithm. A regular mesh is applied to the physical space $\{x, y, z, t\}$. The nodes are numbered by integers ξ, η and σ, and the equations are solved in the transformed space $\{\xi, \eta, \sigma, \tau\}$. The Euler solver in a Flux Vector Splitting algorithm according to van Leer. The solution algorithm is

$$\begin{aligned}\mathbf{q}^{n+1}_{\xi,\eta,\sigma} = \mathbf{q}^{n}_{\xi,\eta,\sigma} \\ &- \Delta t(\mathbf{f}^{+}_{\xi,\eta,\sigma} - \mathbf{f}^{+}_{\xi-1,\eta,\sigma} + \mathbf{f}^{-}_{\xi+1,\eta,\sigma} - \mathbf{f}^{-}_{\xi,\eta,\sigma} \\ &+ \mathbf{g}^{+}_{\xi,\eta,\sigma} - \mathbf{g}^{+}_{\xi,\eta-1,\sigma} + \mathbf{g}^{-}_{\xi,\eta+1,\sigma} - \mathbf{g}^{-}_{\xi,\eta,\sigma} \\ &+ \mathbf{h}^{+}_{\xi,\eta,\sigma} - \mathbf{h}^{+}_{\xi,\eta,\sigma-1} + \mathbf{h}^{-}_{\xi,\eta,\sigma+1} - \mathbf{h}^{-}_{\xi,\eta,\sigma}). \end{aligned} \tag{26}$$

The split fluxes $\mathbf{f}^{+}$ and $\mathbf{f}^{-}$ are defined as follows:

$$\mathbf{f}^{\pm} = D|\nabla\xi|\xi^{\pm}_{m}\begin{Bmatrix} 1 \\ \hat{\xi}_x\dfrac{-u_n \pm 2a}{\kappa} + u \\ \hat{\xi}_y\dfrac{-u_n \pm 2a}{\kappa} + v \\ \hat{\xi}_z\dfrac{-u_n \pm 2a}{\kappa} + w \\ f_e^{\pm} \end{Bmatrix}, \tag{27}$$

where

$$|\nabla\xi| = \sqrt{\xi_x^2 + \xi_y^2 + \xi_z^2}, \quad f_m^{\pm} = \pm\frac{1}{4}\rho a(M_\xi \pm 1)^2, \tag{28, 29}$$

$$f_e^{\pm} = f_m^{\pm}\left[\frac{-(\kappa-1)u_n^2 \pm 2(\kappa-1)u_n a + 2a^2}{\kappa^2 - 1} + \frac{1}{2}(u^2 + v^2 + w^2) - \hat{\xi}_t\frac{-u_n \pm 2a}{\kappa}\right], \tag{30}$$

$$M_\xi = u_n/a, \quad u_n = \hat{\xi}_x u + \hat{\xi}_y v + \hat{\xi}_z w + \hat{\xi}_t, \tag{31, 32}$$

$$(\hat{\xi}_x, \hat{\xi}_y, \hat{\xi}_z, \hat{\xi}_t) = \frac{1}{|\nabla\xi|}(\hat{\xi}_x, \hat{\xi}_y, \hat{\xi}_z, \hat{\xi}_t), \quad D = |\partial(x, y, z)/\partial(\xi, \eta, \sigma)|. \tag{33, 34}$$

The definition of the split fluxes in the η- and σ-directions can be obtained by replacing ξ with η and σ.

The above form (27) of the split fluxes $\mathbf{f}^{\pm}$ is to be used only if $|M_\xi|$ is less or equal 1. Otherwise, $\mathbf{f}^{+} = \mathbf{f}, \mathbf{f}^{-} = \mathbf{0}$ for $M_\xi > 1$, or $\mathbf{f}^{+} = \mathbf{0}, \mathbf{f}^{-} = \mathbf{f}$ for $M_\xi < -1$. More details on the method can be found, for instance, in Parpia (1988).

In addition, utilizing the MUSCL-principle (van Leer 1979), variable extrapolation is applied in order to achieve better spatial accuracy. The boundary conditions at the far field are obtained using one-dimensional approximations of the characteristic equations (Riemann variables). On the wing surface, a combination of extrapolations and the normal momentum equation is applied (Hirsch 1990).

For our computations, we use an annular wing which is created by rotating a NACA6512 profile. D/L equals 1, where D is measured at the foremost edge of the profile. The mesh, for

which an H-topology is chosen, is generated according to the method of Steger & Sorensen (Carstens 1988). There are 116 cells in the ξ-direction, 50 of them upon the profile, and 43 cells in the radial direction, 13 of them inside of the annular wing. The circumference is subdivided into 24 segments.

4. RESULTS

4.1. Steady Flow

All calculations in this section are done with the rotated NACA 6512 annular wing ($D/L = 1$) described in the foregoing. Figure 2 shows iso-Machlines for a typical transonic case at $Ma_\infty = 0{\cdot}8$. The diameter of the duct in the fore part of the nacelle increases in the downstream direction which avoids an acceleration of the flow and the occurrence of possible shock waves on account of nozzle effects. The Mach number directly in front of the shock on the outer side equals 1·32.

At first, the lift polar is considered, i.e. the lift as a function of the angle of attack α. In Figure 3, the annular wing is compared with a 2-D NACA0012 profile at the transonic Mach number of 0·8. The NACA0012 profile was chosen instead of the NACA6512 for this comparison, because the former is symmetric like the annular wing. A 2-D NACA6512 profile is cambered and thus has a nonzero lift at an angle of attack of 0°, in contrast to the annular wing. From Figure 3, it can be seen that the lift is linearly dependent on α for the annular wing. This remains valid even at higher values of α, where the 2-D airfoil already

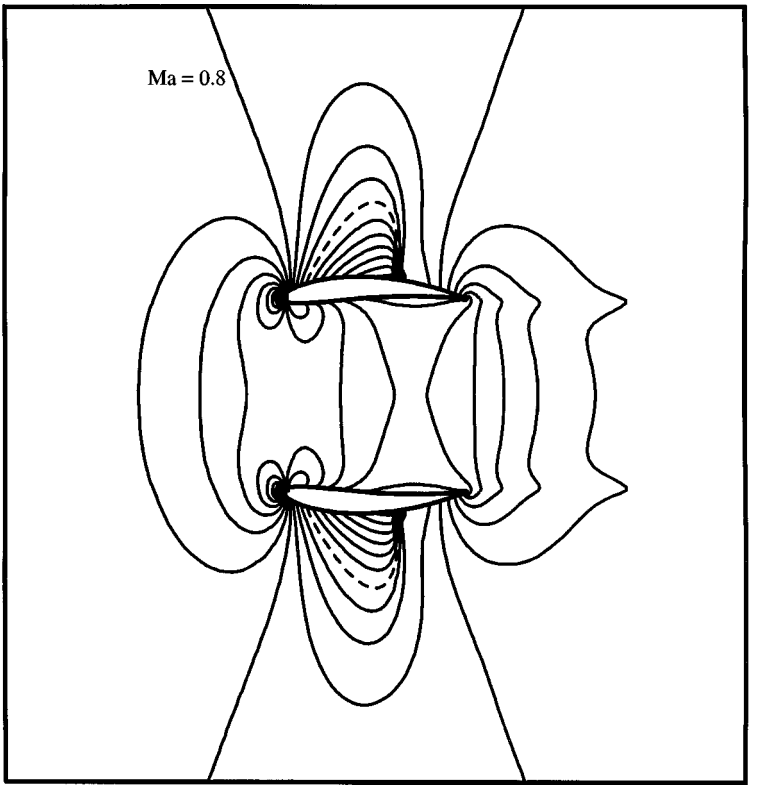

Figure 2. Isomachlines at $Ma_\infty = 0{\cdot}8$, $\Delta Ma = 0{\cdot}05$.

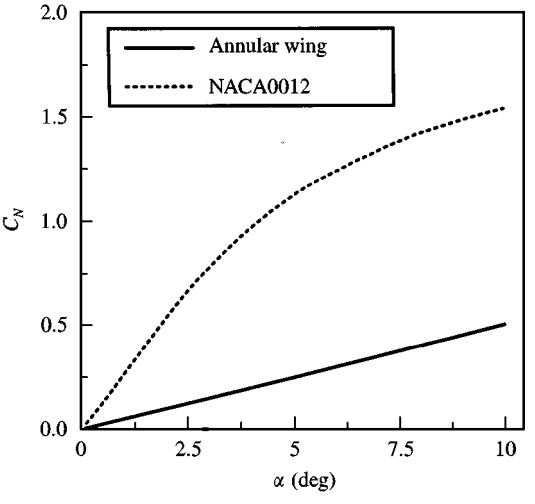

Figure 3. Lift as a function of the angle of attack α for the annular wing (solid) and the NACA0012-profile (dotted) at $\mathrm{Ma}_\infty = 0{\cdot}8$ in steady flow.

shows nonlinear effects. This distinct behaviour can be explained by the channeling effect of the annular wing being responsible for a reduction in the effective angle of attack. It is so small that the lift is linearly dependent on the angle of attack even at higher values of α.

The next parameter to be investigated is the influence of compressibility. Figure 4 shows the steady lift and moment coefficient as a function of $\mathrm{M}a_\infty$. The Mach number dependence is weak and especially less significant than in the case of the high-aspect-ratio airfoil. This result is already predicted by potential theory, but is also valid in the transonic flow regime, where linearized potential theory is no longer applicable. A similar behaviour is known from slender-body theory, where the steady lift remains independent of compressibility effects from $\mathrm{M}a_\infty = 0$ to supersonic conditions. According to Prandtl *et al.* 1990, slender-body theory yields good results for $(1 - \mathrm{M}a_\infty)D^2/L^2 < 0{\cdot}25$. For the annular wing with $D/L = 1$, this is fulfilled only for Mach numbers higher than 0·87, but, obviously, slender-body theory seems to be a good approximation also for lower Mach numbers.

Thus, steady air-loads vary significantly less for annular wings with $D/L < 1$ than for airfoil profiles. In the next section, the question of whether or not this is also true in unsteady flows will be examined.

4.2. Unsteady Flow

The frequencies investigated are $\omega^* = 0{\cdot}25$, 0·5, 0·75, and 1. Higher frequencies practically never occur and the air-loads for $0 < \omega^* < 0{\cdot}25$ can be found by inter polating using the steady air-loads. A typical example of a medium range transport aeroplane could be $\omega = 10\ \mathrm{m/s}^{-1}$ and $L = 3\ m$. This corresponds at $U_\infty = 200$ m/s to a reduced frequency of 0·15. For smaller aeroplanes, the reduced frequencies can be higher, because of the higher frequencies of the structural oscillation modes.

Figure 5 shows the unsteady air-loads in the transonic regime for pitch oscillations. For $\omega^* < 0{\cdot}5$, transonic effects cannot be observed. The real parts correspond to the static derivatives and the imaginary parts remain small. At $0{\cdot}5 < \omega^* < 1$, the real parts of the lift coefficient exhibit a slight increase followed by a decrease, while the imaginary parts

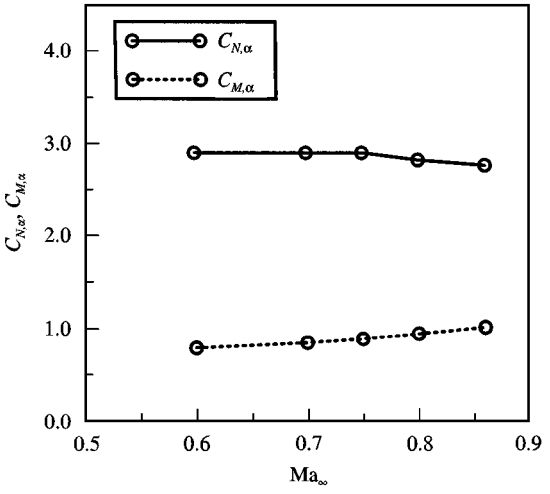

Figure 4. Lift and moment as a function of Ma_∞ for the annular wing in steady flow.

decrease when shifting to transonic Mach numbers. The moment coefficients do not vary significantly.

In Figure 6, the results of the computations are shown for heave oscillations. Again, for $\omega^* < 0{\cdot}5$, transonic effects practically cannot be observed. At higher values of ω^*, all derivatives show minor variations.

Summarizing, steady and unsteady air-loads, acting on an annular wing with $D/L < 1$ in transonic flow, do not differ significantly from their subsonic values. That means, that they behave more benignly than in the case of an airfoil. This can be explained partly by the fact that annular wings can be treated like slender bodies; thus, the compressibility effects can be neglected in the lowest order. Another important point is the channeling effect of the annular wing, which reduces the effective angle of attack.

5. AEROELASTIC STABILITY

The air-loads, calculated in the preceding section, do not vary dramatically while shifting to transonic Mach numbers. Nevertheless, the stability effects of these changes will be investigated, because it is known that, under unfavourable circumstances, aeroelastic stability can be sensitive to several parameter variations.

The aeroelastic model is pictured in Figure 7. Two degrees of freedom are allowed, namely heave and pitch oscillations. The equations of motion are

$$m\ddot{h} + S_\alpha \ddot{\alpha} + D_h \dot{h} + K_h h = -A(t), \tag{35}$$

$$S_\alpha \ddot{h} + I_\alpha \ddot{\alpha} + D_\alpha \dot{\alpha} + K_\alpha \alpha = M(t), \tag{36}$$

where m is the total mass, $S_\alpha = msl$ is the static unbalance, I_α is the moment of inertia, D_h and D_α are damping coefficients, and K_h and K_α are the spring constants. If the air-loads A and M are not explicitly dependent on time and linear functions of h, $\dot{h}$, α, and $\dot{\alpha}$, this system of equations has solutions of the form

$$\begin{Bmatrix} h_1 \\ \alpha_1 \end{Bmatrix} e^{i\lambda t}, \tag{37}$$

where λ, h_1, and α_1 are complex. It is assumed that the system is not degenerate.

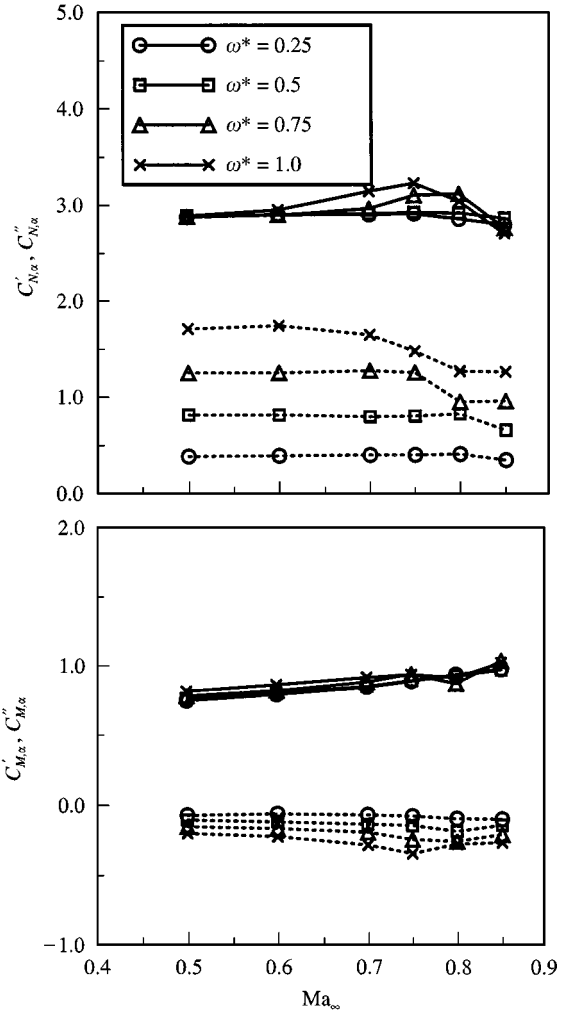

Figure 5. Unsteady load coefficients as a function of Ma_∞ for pitch oscillations :—, real parts; ---, imaginary parts.

The motion is damped if $\mathcal{I}m(\lambda)$ is positive and sustained if negative. Thus, the stability boundary is defined by $\mathcal{I}m(\lambda) = 0$, where the solution oscillates harmonically with constant amplitude. At these points, lift and moment can be calculated utilizing the load coefficients from the preceding section:

$$\bar{A} \propto [(c'_{N,h} + ic''_{N,h})\bar{h}_1 + (c'_{N,\alpha} + ic''_{N,\alpha})\bar{\alpha}_1]e^{i\lambda t}, \tag{38}$$

$$\bar{M} \propto [(c'_{M,h} + ic''_{M,h})\bar{h}_1 + (c'_{M,\alpha} + ic''_{M,\alpha})\bar{\alpha}_1]e^{i\lambda t}, \tag{39}$$

The bar signals that these formulae refer to oscillations around the middle axis B. The transformation to oscillations around the axis D is given by

$$\bar{h} = h - \varepsilon l\alpha, \quad \bar{M} = M - \varepsilon lA, \tag{40, 41}$$

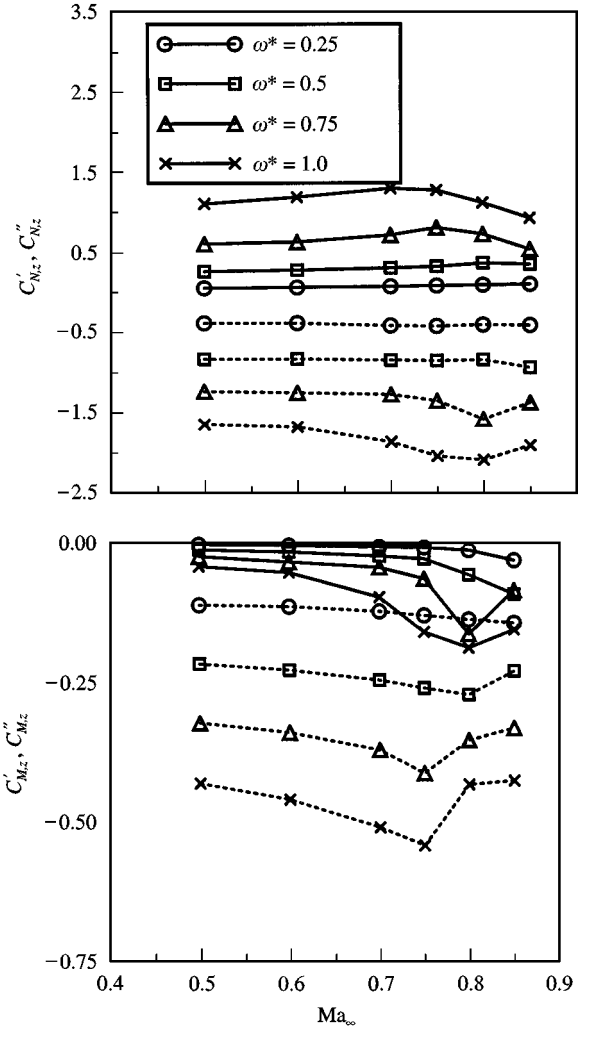

Figure 6. Unsteady load coefficients as a function of Ma_∞ for heave oscillations :—, real parts; ---, imaginary parts.

where ε is the distance of the torsion axis D from the middle axis B. For simplicity damping is assumed to have the form

$$D_h = \frac{\gamma_h K_h}{\omega} \quad \text{and} \quad D_\alpha = \frac{\gamma_\alpha K_\alpha}{\omega}, \tag{42}$$

with constant γ_h and γ_α.

Then, the system of equations (35) and (36) yields the following determining equation for λ:

$$E_{11}\frac{h}{l} + E_{12}\alpha = 0, \quad E_{21}\frac{h}{l} + E_{22}\alpha = 0, \tag{43, 44}$$

with

$$E_{11} = \mu\left(1 - \frac{\omega_h^2}{\omega_\alpha^2}\frac{\omega_\alpha^2}{\lambda^2}(1 + \mathrm{i}\gamma_h)\right) - \frac{1}{\omega'^2}k_a, \tag{45}$$

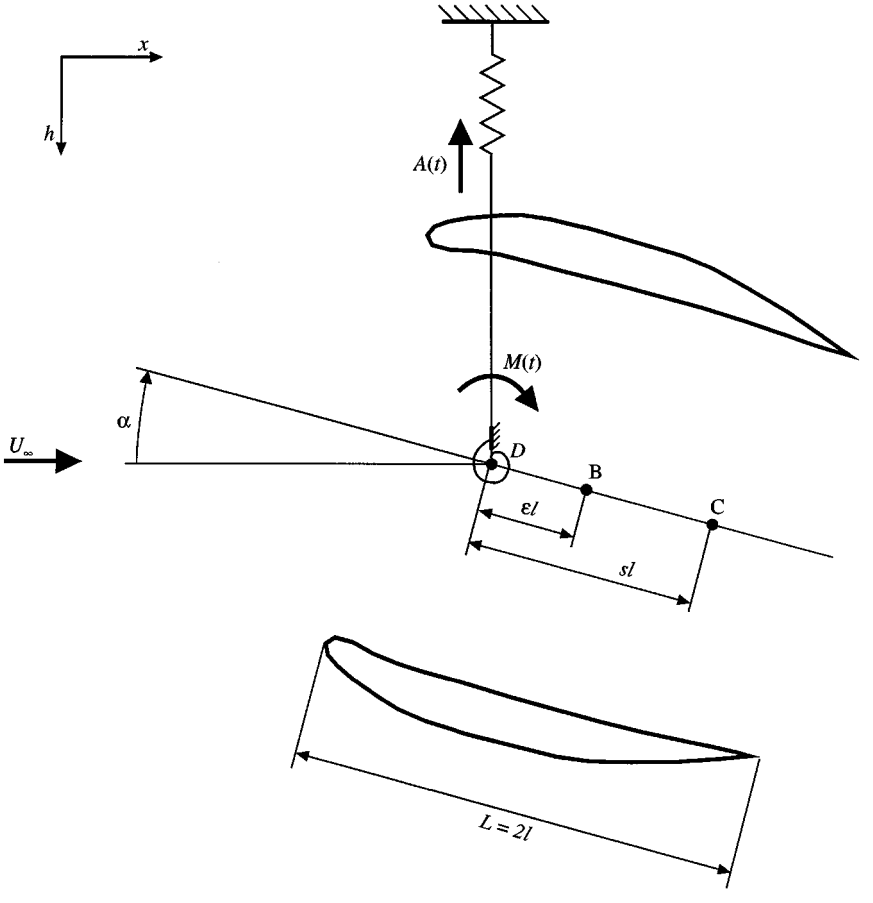

Figure 7. Two-degree-of-freedom (pitch/heave) aeroelastic model.

$$E_{12} = x_\alpha \mu - \frac{1}{\omega'^2}(k_b - \varepsilon k_a), \tag{46}$$

$$E_{21} = \frac{x_\alpha \mu}{2} + \frac{1}{\omega'^2}\left(m_a + \frac{\varepsilon}{2} k_a\right), \tag{47}$$

$$E_{22} = \frac{r_\alpha^2 \mu}{2}\left(1 - \frac{\omega_\alpha^2}{\lambda^2}(1 + \mathrm{i}\gamma_\alpha)\right) + \frac{1}{\omega'^2}\left(m_b + \left(\frac{k_b}{2} - m_a\right) - \frac{\varepsilon^2}{2} k_a\right). \tag{48}$$

In the aeroelastic literature, all mechanical quantities usually are referred to $l = L/2$. This also applies for the reduced frequency. In order to avoid confusion, it is therefore denoted by ω' in this section; $\omega' = \omega l/U_\infty$, $\omega_h^2 = K_h/m$, $\omega_\alpha^2 = K_\alpha/I_\alpha$, $\mu = m/\pi\rho D l^2$, $x_\alpha = S_\alpha/ml$, $r_\alpha^2 = I_\alpha/ml^2$, $k_\alpha = -(c'_{N,z} + \mathrm{i}c''_{N,z})$, $k_b = c'_{N,\alpha} + c''_{N,\alpha}$, $m_a = -(c'_{M,z} + \mathrm{i}c''_{M,z})$, $m_b = c'_{M,\alpha} + \mathrm{i}c''_{M,\alpha}$. The parameters were chosen as $x_\alpha = 0{\cdot}2$, $\mu = 25$, $r_\alpha^2 = 0{\cdot}5$ and $\gamma_h = \gamma_\alpha = 0{\cdot}05$. These are taken from Försching (1991) and are typical for a lightweight annular wing.

Equation (43) has nontrivial solutions only if $E_{11}E_{22} - E_{12}E_{21} = 0$. By this condition $e := \omega_\alpha^2/\lambda^2$ can be obtained easily as a root of a quadratic complex equation. The flutter

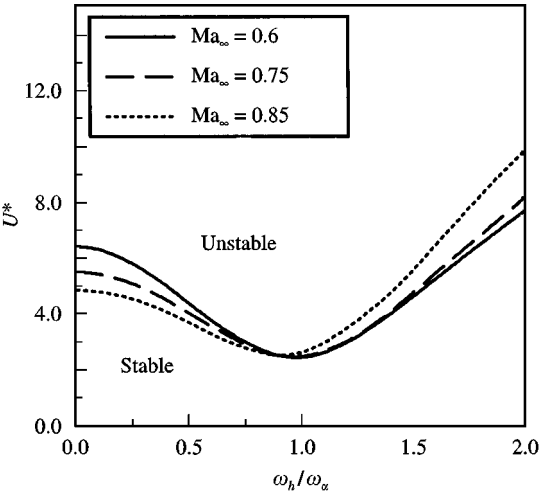

Figure 8. Reduced flutter speed U^* as a function of the frequency ratio at subsonic and transonic Mach numbers for $\varepsilon = -0{\cdot}5$.

points are found by varying ω' and marking the points where $\mathcal{I}m(1/\sqrt{e}) = 0$. Then $\lambda = \omega_F$ is real and can be used to calculate the reduced flutter speed,

$$U_F^* = \frac{U_F}{\omega_\alpha l} = \frac{1/\sqrt{e}}{\omega'}. \tag{49}$$

A typical stability diagram is plotted in Figure 8 for $\varepsilon = -0{\cdot}5$. The flutter speed U_F^* is sketched against the frequency ratio ω_h/ω_α for a subsonic Mach number of 0·6 and transonic Mach numbers 0·75 and 0·85. The unstable region is above the stability curve. The curves imply that for $\omega_h/\omega_\alpha < 1$ transonic effects tend to destabilize the motion; for higher ratios, they have a stabilizing character. This statement does not hold globally, but refers only to this combination of parameters. At other values, the consequences of the transonic effects can be different. However, systematic parameter studies are not necessary because, in the case of a pylon-mounted engine, pure nacelle flutter cannot occur. This is because the centre of gravity normally lies far ahead of the flexure axis. Therefore, the aim of the present flutter calculation is to demonstrate that transonic effects at the annular wing are principally able to destabilize the system. This statement is of special interest, because the combined airfoil-nacelle modes are essential for some practical flutter cases.

6. JET SIMULATION

The simulation of the jet is an important step on the way towards a realistic engine model. For Euler calculations, this can be achieved by using an actuator disk method [see e.g. Rudnik (1991), Hirose *et al.* (1991) or Chen *et al.* (1983)]. In this study, this is implemented using a combination of the characteristic equations (16)–(21) and fixed boundary conditions. This steady method is expanded in such a way that unsteady flows can be treated.

The coordinates of the annular wing used for the jet simulation can be found in Knipfer (1995). The profile is thinner and less cambered than the NACA6512 profile used in the preceding sections; D/L equals 0·7. Ma_∞ is kept at 0·6 in order to avoid transonic effects.

6.1. Steady Flow

At the fan inlet, the characteristic equation (20) which describes an upstream running wave, is replaced by the condition of constant mass flow density j_F; j_F is set to 60% of the mass flow density at infinity. This value is slightly higher than the average value for the pure flow-through nacelle (56%) in order to take account of the working fan. At the fan outlet, equations (16)–(19), which describe waves running in the downstream direction, are replaced by the conditions of constant mass flow j_F, total pressure ratio $p_t = p_{0,\mathrm{fan}}/p_{0,\infty}$ and flow directions θ_1 and θ_2; θ_1 and θ_2 are respectively the polar and the azimuthal angle of the velocity vector, both set to zero. p_t is varied from 1 (no thrust) to 1·3. Figure 9 shows iso-Machlines for $p_t = 1{\cdot}3$. The shear layer indicating the jet boundary can be clearly identified. It is widened in the downstream direction on account of numerical viscosity.

6.2. Unsteady Flow

The method of fixed boundary conditions as described in the foregoing is not appropriate for unsteady flow because the front and the rear sides of the fan are completely decoupled. Thus, for unsteady flow, waves must be allowed to cross the actuator disk. In the following, two methods are introduced and tested.

In both cases, the simulation starts with a converged steady solution. In order to determine the unknown variations of the 10 variables $\delta_{p\mathrm{front}}$, $\delta_{p\mathrm{front}}$, $\delta u/v/w_{\mathrm{front}}$ *and* $\delta_{p\mathrm{rear}}$, $\delta_{p\mathrm{rear}}$, $\delta u/v/w_{\mathrm{rear}}$, 10 equations are needed. Five of them are the characteristic equations for the incoming waves. They yield four relations for the variables on the foreside of the fan and one for the backside. The two methods differ in the manner of obtaining the missing equations. Method 1 is based on the assumption that incoming waves cross the fan undisturbed, i.e., the variations of the characteristic variables are equal fore and aft of the actuator disk. This can formally be expressed by

$$[\Delta s_i] = 0; \tag{50}$$

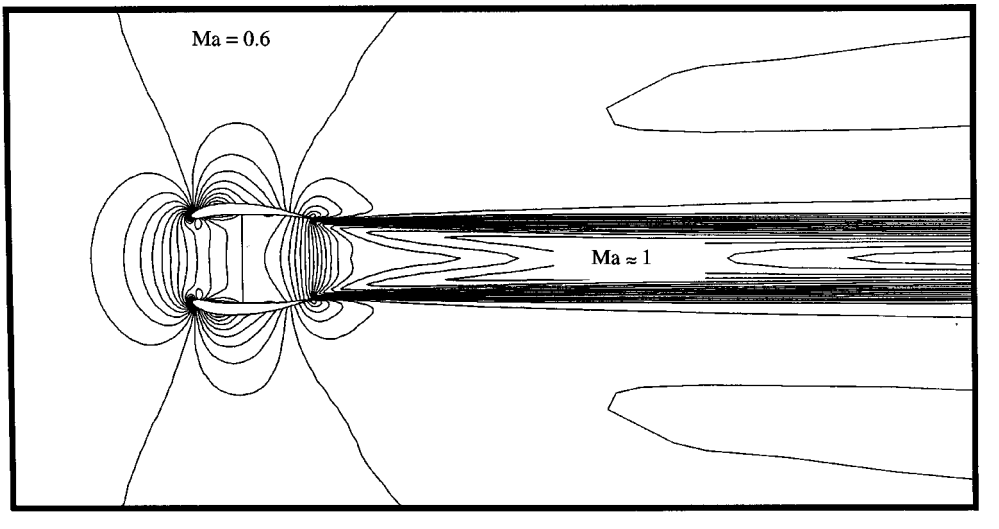

Figure 9. Isomachlines for $\mathrm{Ma}_\infty = 0{\cdot}6$ and $p_t = 1{\cdot}3$ ($\Delta\mathrm{Ma}_\infty = 0{\cdot}025$).

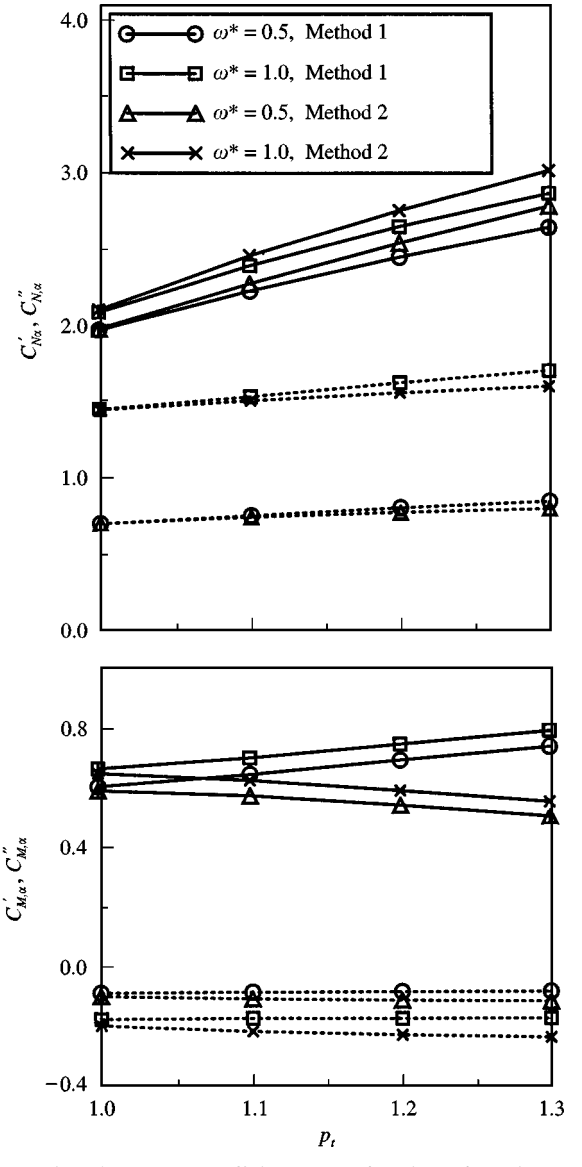

Figure 10. Unsteady normal and moment coefficients as a function of total pressure jump p_t for pitch oscillations :——, real parts; ---, imaginary parts.

[ ] means the difference between the values at the front part and at the backside of the fan. In method 2, it is demanded that the jump relations across the fan are conserved:

$$\frac{\partial}{\partial t}[\rho u] = 0, \quad \frac{\partial}{\partial t}[\rho u^2 + p] = 0, \tag{51, 52}$$

$$\frac{\partial}{\partial t}[\rho uv] = 0, \quad \frac{\partial}{\partial t}[\rho uw] = 0, \quad \frac{\partial}{\partial t}[\rho uI] = 0. \tag{53, 54, 55}$$

The variables do not vary greatly from one integration step to the next, so these equations can be used in their linearized form.

The computations yield the result that for heave oscillations unsteady air-loads $c_N/c_{M,z}$ are almost completely independent of the jet strength p_t (not shown). This can be explained by the fact that there is no motion of the annular wing normal to the pressure jump at the fan. For pitch oscillations, the results of the two methods are plotted in Figure 10. Real parts of the lift become significantly stronger, which usually corresponds to less stable aeroelastic behaviour. With the exception of the real parts of the moment, the results for both methods are almost identical. No simple explanation for this distinct behaviour could be found. However, it has to be kept in mind that the absolute values of the moments are relatively small.

Other methods can be defined as hybrids between the two methods. Furthermore, reflection or transmission coefficients can be introduced. In order to calibrate these methods, detailed experimental results are needed which answer the question of what happens to a wave crossing a working fan.

7. SUMMARY

The main issue investigated in this paper has been the influence of nonviscous transonic flow on unsteady load coefficients, acting on an oscillating annular wing with aspect ratio $D/L = 1$.

The steady load coefficients do not vary with the Mach number, i.e., transonic effects do not occur. Thus, the annular wing with $D/L = 1$ can still be regarded as a slender body. The unsteady load coefficients do not depend on the Mach number for reduced frequencies of less than 0.5. At higher frequencies, transonic effects remain in a range of 10%. The relative shifts of the stability curves have the same order of magnitude; this is only valid for the isolated annular wing. If the pylon and the airfoil are taken into account, it is known by experiments that shocks are able to cause severe stability problems for the system wing-pylon-engine. Thus, a next step would be to include wing and pylon and to take into account the viscous effects.

In addition, two methods for an unsteady jet simulation have been developed. Both methods yield almost the same dependence of the unsteady air-loads on the pressure jump. In order to refine the methods, wind tunnel experiments are needed.

References

Angelini, J. J., Chopin, S. & Destuynder, R. 1974 Forces aerodynamiques instationnaires induites par les vibrations aeroélastiques d'un réacteur en nacelle. *Recherche Aerospatiale* **4,** 209–219.

Bolms, H.-TH, Schwamborn, D. 1994 Numerical solution of the flow around a turbofan and its wind tunnel simulator. *ICAS*-94-3.7.2., pp. 2400–2408.

Carstens, V. 1988 Two-dimensional elliptic grid generation for airfoils and cascades. DLR-Forschungsbericht 88–52.

Chen, H. C., Yu, N. J. & Rubbert, P. E. 1983 Flow simulations for general Nacelle configurations using Euler equations AIAA Paper 83–0539.

Försching, H. & von Dienst, K. 1991 Flutter stability of annular wings in incompressible flow. *Journal of Fluids and Structures* **5,** 47–67.

Hirose, N., Asai, K., Ikawa, K. & Kawamura, R. 1991 Euler flow analysis of turbine powered simulator and fanjet engine *Journal of Propulsion and Power* **7,** 1015–1022.

Hirsch, Ch. 1990 *Numerical Computation of Internal and External Flows*, Vol. 2, pp. 379–384. Chichester: Wiley.

Katzer, E. 1989 Stationäre und instationäre Potentialströmung um dünne Ringflügel und Triebwerke mit Simulation des Triebwerkstrahls DLR-Forschungsbericht 89.

Knipfer, A. 1995 Numerische Untersuchung der transsonischen Strömung an schwingenden Triebwerksgondeln. DLR-Forschungsbericht 95–39.

Laschka, A. 1964 Über die Potentialtheorie von zylindrischen rotationssymmetrischen Flügeln (Ringflügel) in kompressibler instationärer Unterschallströmung. *Zeitschrift für Flugwissenschaft* **12,** 205–211.

Parpia, I. 1988 van Leer flux vector splitting in moving coordinates. *AIAA Journal* **26,** 113–115.

Prandtl, L., Oswatitsch, K. & Wieghardt, K. 1990 Führer durch die Strömungslehre, p. 474. Braunschweig: Vieweg.

Ronzheimer, A. 1989 Erweiterung eines Euler-Verfahrens zur Strömungsberechnung um dreidimensionale Gondeln mit hohem Bypass-Verhältnis. DLR-Institutsbericht 129–89/42.

Rudnik, R. 1991 Erweiterung eines dreidimensionalen Euler-Verfahrens zur Berechnung des Strömungsfeldes um Nebenstromtriebwerke mit Fan- und Kernstrahl. *Zeitschrift für Flugwissenschaft und Weltraumforschung* **15,** 285–288.

Schlichting, H. & Truckenbrodt, E. 1969 *Aerodynamik des Flugzeuges* 2, p. 159. Berlin: Springer-Verlag.

Send, W. 1989 Unsteady lift and moment coefficients of an engine Nacelle. In 'Proceedings of the European Forum on Aeroelasticity and Structural Dynamics. DGLR-Bericht 89-1, pp. 159–168.

van Leer, B. 1979 Towards the ultimate conservative difference scheme. V. A second-order sequel to Godunov's method. *Journal of Computational Physics* **32,** 101–136.

Weissinger 1956 Zur Aerodynamik des Ringflügels. *Zeitschrift für Flugwissenschaft* **4,** 141–150.